Progress of the XFEL Project

1. Status of XFEL Construction

A five-year construction project for an 8-GeV XFEL facility, which was started in FY2006 as one of the Key National Technologies in Japan, went well in FY2010, the final year of the construction. The manufacture of all the components was completed so full power rf aging started in October 2010.

We have completed the development of beam commissioning procedures and tools necessary for the XFEL beam commissioning. One of the most difficult developments was the modeling of the XFEL linear accelerator, which is essential for precise beam control achieving a high peak current of more than 3 kA. The model developed can consistently describe the transverse electron beam envelope and beam peak current at the lasing slice over the XFEL, i.e., from the electron gun cathode to the 8-GeV beam dump. Another difficult development was the design of a precise alignment method for a long undulator beamline over 100 m, of which the maximum allowed deviation from a reference straight line is ±4 mm. The beam-based method developed can satisfy the requirement without any iterative procedure. On the basis of the elaborate investigation, we have successfully prepared all the high-level software programs in order to perform the beam tuning required for stable high-power SASE XFEL. The beam commissioning was start on 21st February towards achieving the first lasing at least before summer 2011. Figure 1 shows the present schedule of the XFEL beam commissioning.

At the XFEL injector, a thermionic electron gun ejects 500-keV electron beam pulses from a CeB_6 cathode and the following bunching section composed of multistage rf cavities bunches and accelerates the beam to form a bunch of 30 MeV energy and 20 ps bunch width. The SCSS test accelerator has shown

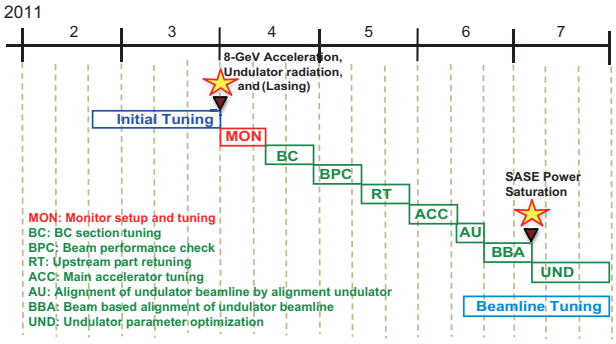

Fig. 1. Schedule of XFEL beam commissioning.

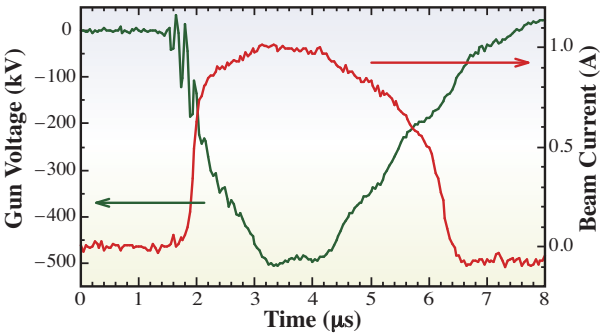

Fig. 2. Observed acceleration voltage pulse and beam current of 500-keV gun.

that this step-by-step bunching scheme promises the realization of the XFEL with its ultralow emittance beams. The installation of the XFEL injector system has almost been realized. The completed electron gun was operated to demonstrate its beam performance at the specified peak current of 1 A, as shown in Fig. 2. The multistage bunching section comprises a 238 MHz subharmonic buncher, a 476 MHz booster, L-band correction cavities, L-band accelerating structures and a C-band correction structure. Their rf powers have reached the required levels after the rf conditioning of every accelerating structure. The two L-band accelerating structures (see Fig. 3) of the alternative periodic structure (APS) type compress the 1-MeV beam bunch and accelerate it up to 35 MeV. A vacuum-type waveguide circuit is employed so as not to use insulation gases such as SF_6, that is, no circulator is available. Therefore, the circuit was carefully designed to cancel the reflected powers from the APSs so that the reflection to the klystron will not cause rf instability in the klystron output cavity [1].

Fig. 3. L-band accelerating structures and their waveguide system.

The acceptable instabilities of the accelerating voltages in the gun and cavities, which permit a 10% rms variation of the peak beam current, are only about 0.01% rms in amplitude and 120 fs rms in phase according to results of the beam simulation. The long-term rf variations can be compensated by the feedback control of the rf amplitude and phase; the short-term or pulse-to-pulse variations, however, have to be reduced as much as possible by improving rf equipment such as amplifiers. Thus, we have carefully designed and manufactured rf cavities, amplifiers and control systems, giving the highest priority to the stabilization of short-term variations. Table 1 shows that the achieved short-term rf stabilities almost satisfy the requirements mentioned above.

We introduced geomagnetic correction coils to cancel the geomagnetic field by a uniform magnetic field to facilitate fine beam tuning at the long low energy section less than 1 MeV. Before the installation of the injector components, we found that the geomagnetic field was strongly distorted by the inhomogeneous magnetism of the reinforcing steel rods in the RC floor and this result suggested that the geomagnetic correction would not function well. We demagnetized the floor using a flat square coil generating an alternating and decaying field. The vertical components of the residual field with subtraction of the genuine geomagnetic field distribute in the range of 0 - 0.05 after the demagnetization, while in the range of –0.1 - 0.5 before it, as shown in Fig. 4.

Immediately after the completion of building construction and geological survey along the 400-m linear accelerator and 200-m undulator hall, the installation of the main accelerator started in Summer 2009. It took one and half years to complete the hardware components, i.e., the 128 C-band accelerator columns (1.8 m long each; Fig. 5), 64 C-band klystrons (Fig. 6), their pulse power supplies,

Table. 1. Tolerances and achievements of short-term accelerating voltage variations

	Tolerance (σ)		Achievement (std.)	
	ΔV/V	Δϕ	ΔV/V	Δϕ
Gun	0.003%	—	0.001%	—
SHB	0.01%	0.01°	—	0.02°
Booster	0.01%	0.02°	0.013%	0.014°
L-Correction	0.03%	0.06°	0.026%	0.062°
L-APS	0.01%	0.06°	0.002%	0.004°
C-Correction	0.1%	0.1°	0.002%	0.004°

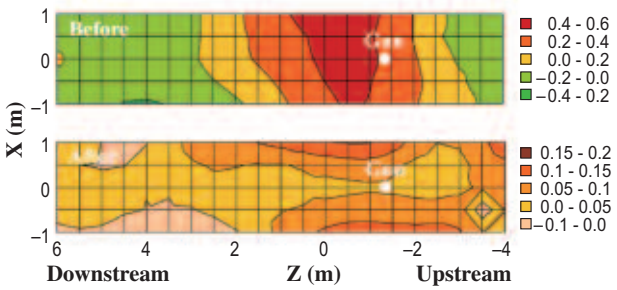

Fig. 4. Vertical magnetic field distribution on horizontal plane at height of beam (80 cm) in injector area before/after demagnetization. The geomagnetic components are subtracted.

and low power rf systems. During the fabrication and installation, we encountered several hardware problems. The most serious one was that the 50-kV PFN capacitor charger with high power switching circuitry underwent frequent breakdowns in resonant capacitors. After careful investigation, the cause was identified to be the gas discharge in the remaining micron-sized gaps among the winding aluminum foils and insulators. By optimizing the capacitor size, interior material and oil immerse process, this problem was successfully solved. Other problems were mostly trivial and were solved properly, and the hardware was successfully installed into the accelerator. From October 2010, we started the high power processing of the S-band (2856MHz) and C-band (5712 MHz) accelerators. After 300 hours of high power operation at 60 pps, the C-band reached 38 MV/m or more, while the S-band required 1000 hours to reach 17 MV/m. We confirmed the superior performance of the C-band system in terms of its high gradient acceleration capability. Some of the C-band klystrons showed multipacting discharge phenomena at lower power operation. Fortunately, it did not cause serious limitation in machine performance. The beam operation is scheduled to start in March 2011, and the first lasing at 1 Å is expected before Summer 2011.

The XFEL/SPring-8 undulator is composed of 18 segments of in-vacuum undulators (IVUs), each of

Fig. 5. C-band acceleration unit installed in accelerator building.

Fig. 6. Modulator and timing systems in klystron gallery.

which has a magnetic period of 18 mm and a magnetic length of 5 m. The maximum K of 2.2 is available at a minimum gap of 3.5 mm. The design of each IVU is based on that of the SPring-8 storage ring with a minor revision to resist the larger mechanical load due to the stronger magnetic field. The construction of the IVUs was started in October 2008 and the construction of the first undulator was completed in October 2009. After the installation in the undulator hall, "*in situ*" field measurement, i.e., the measurement of the field distribution in the vacuum chamber, was carried out to check the magnetic quality variation during the assembly process in the field measurement facility and the transport to the XFEL facility. The field errors found in the measurement were corrected by finely adjusting the gaps at several positions along the undulator axis. Regardless of minor problem concerning vacuum components, the construction, installation, and *in situ* field measurement of all the undulator segments were completed by the end of August 2010 on schedule except for the installation of a few components. Figure 7 shows a photograph of the 18 segments installed in the undulator hall taken from the downstream side.

The installation of basic beam instruments, such as beam position monitors (BPM), current transformer (CT), and screen monitors (SCM), in the XFEL building proceeded after mass production of the instruments [2]. By the end of 2010, the installation was almost finished. Figure 8 shows the current state of the installation of the BPM and CT. Even though the installation is almost complete this year, we still have a problem that needs to be solved with a new idea, namely, the difficulty in measuring the position of a very horizontally flat beam shape in the energy-dispersive part, such as a bunch compressor chicane, and in observing a bunch length in the femtosecond region. Therefore, a multi-stripline beam position monitor (M-BPM) [3] with five 50 Ω striplines placed along a horizontal cross section for observing a beam position at the energy dispersive part was developed. This monitor can observe not only the mass center of a beam intensity distribution along a transverse direction, but also its rough distribution. Position sensitivity, as shown in Fig. 9, was measured at the SCSS test accelerator using a prototype M-BPM with three striplines. This sensitivity is sufficient for the beam tuning of the XFEL. For the bunch length measurement, monitor systems using optical transition radiation (OTR) observed with a streak camera, coherent synchrotron radiation (CSR) observed with

Fig. 7. Installed 18 IVU segments.

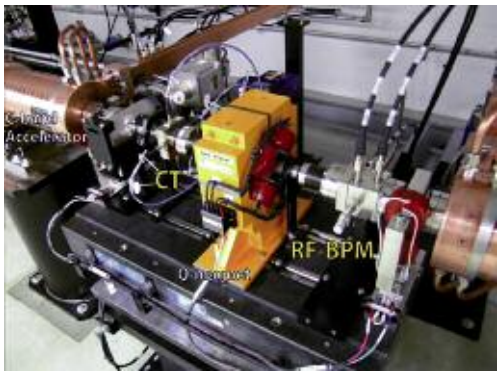

Fig. 8. BPM and CT installed in accelerator tunnel.

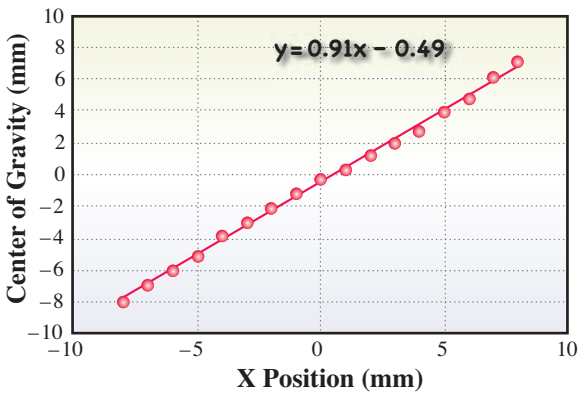

Fig. 9. Horizontal beam position dependence of gravity center of M-BPM signal. A linear function fitted to the data is also plotted.

a pyrodetector, and coherent transition radiation observed with a waveguide spectrometer have been developed [4].

The mass production of timing and low-level rf components, such as in-phase, quadrature phase and amplitude (IQ) detectors and modulators, as well as 600 W solid-state amplifiers for driving 50 MW high-power klystrons operated at the L- (1428 MHz), S- (2856MHz), and C- (5712 MHz) bands, was almost completed in the beginning of 2009 [5]. Furthermore, an optical time-reference signal transmission system, comprising a master oscillator, optical fiber cables, and electrical/optical and optical electrical converters using 1550 nm laser diodes and pin-photo diodes, for driving klystrons was fabricated [5,6]. After this mass production, all the instruments were installed into water cooling 19 inch racks; these racks were set in the XFEL building in 2009. At the end of 2009, the installation of the racks was almost finished, and rf conditioning for accelerating structures was started in December using these racks and an optical time-reference transmission system. During the rf conditioning operation, the racks and signal transmission system worked well without any major problems. Figure 10 shows the side-band noise level of a 5712 MHz carrier signal measured at the output of the system. This low-noise level of -150 dBc at a 1 MHz offset frequency is clear evidence of the soundness of our installed system.

The electromagnets of the XFEL/SPring-8 consist of 10 magnetic lenses (2 types), 114 quadrupole magnets (5 types), 121 steering magnets (5 types) and 28 bending magnets (7 types). Different from those of a storage ring, their magnetic fields and sizes should be increased with the beam energy along the linac. Therefore, a wide variety of magnet types are required. Since most of the magnets are operated by DC, pure iron blocks are used as a yoke material to reduce production cost except steering magnets. The installation of the magnets was completed by Summer 2010. Figure 11 shows a 6.7-m-long bending magnet installed before the 8 GeV beam dump. The magnetic fields of important magnets were remeasured after its installation in the accelerator tunnel. To avoid the hysteresis of iron yokes, the magnets are excited using a fixed current pattern. A magnetic field reproducibility on the order of 10^{-4} is attained with the pattern excitation. Since the steering magnets will be used for an orbit feedback system, their yokes are made of permalloy to reduce hysteresis. A field reproducibility of about 10^{-4} has been achieved for the steering magnets without any initialization or pattern excitation processes. The magnet power supplies are controlled by a VME-based optical linked I/O system. A remote VME card (i-DIO) is installed in a power supply chassis and one i-DIO card controls two output channels. An FPGA is also mounted in the i-DIO card, which evaluates and provides the status of the power supply for interlock systems.

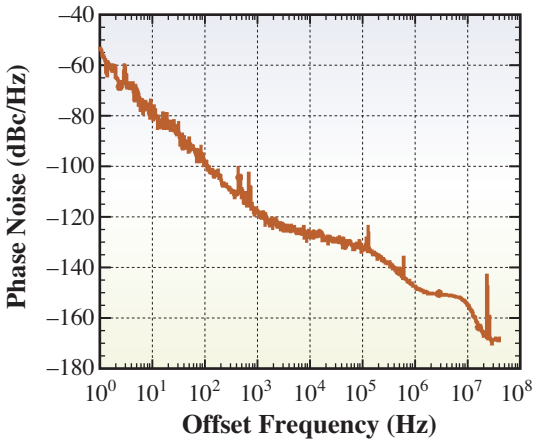

Fig. 10. Phase noise spectrum of 5712 MHz output signal from optical electrical converter installed at CB05-4 unit.

Fig. 11. Bending magnet installed before final beam dump.

The vacuum component assembly and installation, cabling installation, leak test and vacuum system operation test were completed in FY2010. The pressures were on the order of 10^{-7} Pa or less. The cold cathode gauge (CCG) arranged near the beamline was inserted into the steel pipe to decrease the leakage magnetic field of its permanent magnet. For the beam-based-alignment technique, the allowable magnetic field upstream of the insertion devices is below 0.4 mG. To decrease the magnetic field, the material of the chamber support was changed from SS400 to SUS316L, and the magnetic field sources such as the sputter ion pump and CCG were placed far from the beam. The vacuum pipes were wrapped with a magnetic shielding sheet. The undulator and the adjacent motion stage on which the electromagnet and the BPM are mounted can move independently. The allowable tolerance of the

bellows connected to their vacuum chambers was 2 mm. The limit switches were set to prevent the bellows from damage caused by large deformation. The limits of the motion along the vertical and horizontal directions were set at ±1.41mm, and the measured repeatability error within a short period was 3 μm.

In the installation and alignment of the XFEL facilities, although the accelerator building is a base of pile foundation supported by a bedrock layer, a 0.1 mm/month subsidence was observed in December 2010 at the midpoint of the building, where the embankment is thickest (50 m). Accelerating structures, BPM, and Q-magnets (Q-Mags) in the building were aligned within ±0.3 mm along a smooth line. The light source building was more stable. For this building, a direct foundation on a bedrock or an artificial layer replaced by excavation with crusher stone was adopted. Insertion devices, BPM and Q-Mags in this building were aligned within ±0.2 mm along a straight line.

An Electron Beam Transport Line was designed to transport a high-quality electron beam from XFEL-Linac to the SPring-8 storage ring (XSBT). The fabrication of all components of the XSBT was completed in March 2010. The installation and final alignment works in the XFEL undulator building were completed in summer 2010. Field measurements for all the bending magnets were completed prior to their installation.

Several key experimental facilities were completed in 2010. After the inauguration of the XFEL Experimental Building in May, four experimental hutches were constructed in the experimental hall (Fig. 12). The beamline components and X-ray optical devices, such as mirrors and double-crystal monochromator (DCM), were installed in the optics hutch. A laser booth for containing the synchronization laser and a timing distribution system were prepared. A beamline for the XFEL-SPring-8 Experimental Facility, which is built for the simultaneous utilization of XFEL and SPring-8 undulator radiation, has also been designed.

Fig. 12. Experimental hutches.

In parallel with the construction works, R&D for XFEL utilization has been performed. In particular, the Plasma Chemical Vaporization Machining (Plasma CVM), which was developed by Osaka University, was used in fabricating thin crystal devices as key components of an X-ray beam splitter. We found that a strain-free, thin window of sub-100 micron thickness is achievable using this technique.

The development of seeding technologies is crucial for upgrading FEL radiation properties and achieving the Fourier-limited pulses. A test experiment was performed at the SCSS test accelerator in close collaboration with RIKEN ASI, JAEA, and the University of Tokyo. A 13th harmonic of a Ti:sapphire (Ti:S) laser in a plateau region was injected as a seeding source into the SCSS. Random and uncontrollable spikes in the Self-Amplified Spontaneous Emission (SASE)-based FEL radiation were found to be strongly suppressed to form a narrow-band, single peak profile at 61.2 nm when the seeding conditions were fulfilled. This technology will be extended to shorter-wavelength regions such as the water-window region between 2 to 4 nm (Fig.13).

In the XFEL experiments, two-dimensional (2D) X-ray detectors optimized for XFEL applications are required to explore the full potential of the XFEL source. As the standard 2D X-ray detector of the facility, the multi-port CCD (MPCCD) detector was developed in March 2009. In 2010, MPCCD sensors and their readout electronics were manufactured and characterized. Detector noise, which is one of the most important performance features, has been demonstrated. The detector assembly for single, dual, and octal sensor detector systems is in progress. Advanced 2D sensor development based on silicon-on-insulator CMOS technology has been carried out. The use of floating-zone wafer has enabled 500-mm-deep depletion. This deep depletion together with back-illumination geometry will improve radiation

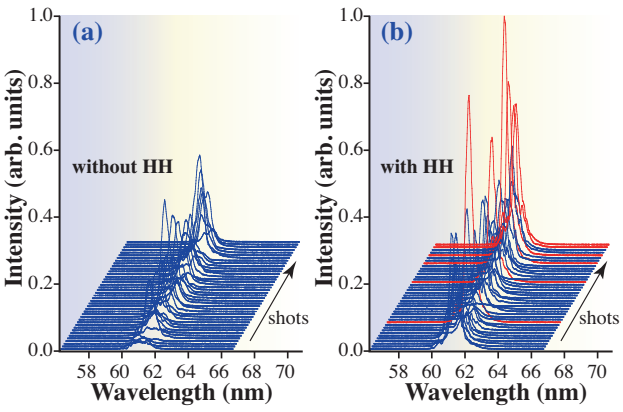

Fig. 13. Comparison of radiation spectra of FEL under unseeded (a) and seeded (red curves in b) conditions.

hardness and quantum efficiency enough to meet the XFEL requirements. After obtaining these results, the development of production detector was started. A data acquisition system for MPCCD, commercial cameras, and waveform digitizers is now being developed. All the data are labeled by trigger numbers and stored by high-speed storage. The development of a DAQ system for the optical hutch and other experimental hutches is now in progress.

2. Operation Status of the SCSS Test Accelerator

After the proof-of-principle experiment showing that an FEL system based on the SCSS concept can generate a high-performance SASE FEL, the test accelerator has been improved aiming at an ideal FEL operation. Despite the day-by-day operation, the continuous power saturation of a SASE FEL has been routinely obtained at wavelengths from 50 to 60 nm. In FY2010 (9 months from April to December), the total beam time is 155 days, and 54% of this or 83 days was provided to user experiments. The regular beam time in a day is currently 9 h from 10:00 a.m. to 7:00 p.m.

2-1. Summary of user experimental programs

In 2010, the EUV-FEL experimental facility accommodated about 100 scientists representing 18 scientific groups not only from Japan but also worldwide, such as Germany, Italy, Netherlands, and Czech Republic. Research using EUV-FEL is carried out in a large variety of disciplines, including technical research preparatory for XFEL experiments, atomic and molecular physics, coherent diffraction imaging methods, damage of optics, materials science, and the science of various devices such as advanced scintillators and nonlinear X-ray devices. The number of publications from the users of EUV-FEL in FY 2010 was ten [i - x].

Here, we show one of the specially chosen research highlights. The group of Hikosaka has observed a multiphoton double ionization in an intense EUV field using shot-by-shot photoelectron spectroscopy [v]. Figure 14 shows photoelectron spectra in the range of the Ar^{2+} $3p^{-2}$ peaks, derived from single-shot basis analysis. The experiment illustrated that the dominant ionization pathway of argon atoms has two steps: first, a single laser photon is absorbed to create singly ionized argon, and then two more photons are absorbed to create doubly ionized argon. In addition, Hikosaka's group found that the intermediate argon ion states have energy levels, or energy resonances, that induce this pathway.

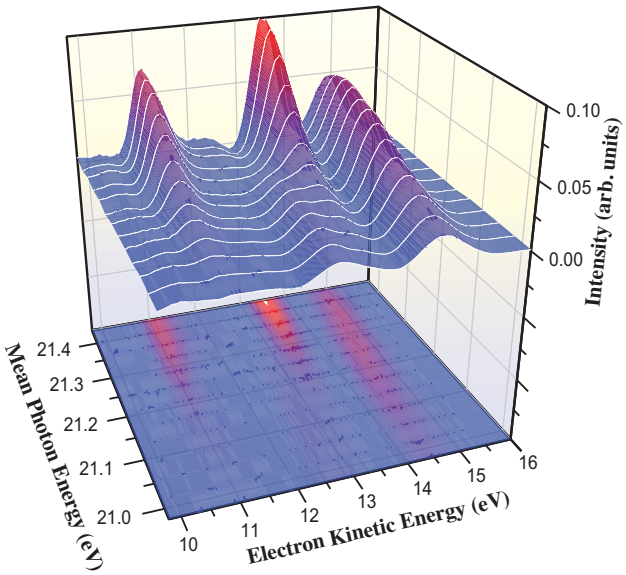

Fig. 14. Photoelectron spectra in range of $Ar^{2+}3p^{-2}$ peaks, derived from single-shot basis analysis.

SPring-8 Joint-Project for XFEL

E-mail: Project-XFEL@riken.jp

References

[1] H. Hanaki *et al.*: Proc. of IPAC'10 (2010) 1722.
[2] S. Matubara *et al.*: Proc. of IPAC'10 (2010) 957.
[3] H. Maesaka *et al.*: Proc. of IPAC'10 (2010) 945.
[4] Y. Otake *et al.*: Proc. of BIW10 (2010) - *in press*.
[5] N. Hosoda *et al.*: Proc. of IPAC'10 (2010) 2191.
[6] T. Ohshima *et al.*: Proc. of IPAC'10 (2010) 1390.

Publication list from the users:

[i] H. Ohashi *et al.*: Nucl. Instrum. Meth. A (2011) - *in press*.
[ii] Y. Nishino *et al.*: Appl. Phys. Exp. **3** (2010) 102701.
[iii] K. Nagaya *et al.*: J. Electron Spectros. Relat. Phenom. **181** (2010) 125.
[iv] M. Kato *et al.*: Metrologia **47** (2010) 518.
[v] Y. Hikosaka *et al.*: Phys. Rev. Lett. **105** (2010) 133001.
[vi] K. Yamanoi *et al.*: Opt. Mater. **32** (2010) 1305.
[vii] H. Iwayama *et al.*: J. Phys. B: At. Mol. Opt. Phys. **43** (2010) 161001.
[viii] A. Yamada *et al.*: J. Chem. Phys. **132** (2010) 204305.
[ix] H. Fukuzawa *et al.*: J. Phys. B: At. Mol. Opt. Phys. **43** (2010) 111001.
[x] S.Y. Liu *et al.*: Phys. Rev. A **81** (2010) 031403(R).